ELSEVIER

Journal of Alloys and Compounds 216 (1994) 75–83

Journal of ALLOYS AND COMPOUNDS

MgB_2C_2, a new graphite-related refractory compound

Michael Wörle, Reinhard Nesper*

Inorganic Chemistry Laboratory, ETH-Zürich, Universitätstr. 6, CH 8092 Zürich, Switzerland

Received 8 March 1994; in final form 30 March 1994

Abstract

MgB_2C_2 is the first structurally well-characterized borocarbide of the alkaline earth metals. The orthorhombic crystal structure ($a = 1092.2$ pm, $b = 946.1$ pm, $c = 745.9$ pm, Cmca-D_{2h}^{18}) contains slightly puckered graphite-related layers $^2_\infty[BC]^-$. The puckering is caused by a specific Mg^{2+} distribution. Only one half of the possible cation sites are occupied, which gives rise to an enhanced ionic conductivity. The compound undergoes topochemical reactions. MgB_2C_2 is a brittle material which crystallizes with thin red transparent platelets.

Keywords: Borocarbides; Alkaline earth metals; Graphite; Ionic conductivity

1. Introduction

Graphite and graphite-related materials have been of enormous interest for many decades owing to the fact that they often combine many desired materials properties, like relative chemical inertness, layer structures, high melting points, and other interesting physical properties [1]. Both the semimetallic graphite itself and the insulating hexagonal boron nitride, the classical Grimm–Sommerfeld variant [2] of graphite, have a large spectrum of technical applications.

Up to now only two compounds have been reported with graphite-like $^2_\infty[BC]$ nets, namely LiBC [3–5] and BC_3 [6]. In the latter compound the BC distribution has not been unambiguously determined experimentally.

A few years ago, the new ternary borocarbide LiBC was synthesized and characterized [3,4]. Its planar $^2_\infty[BC]^-$ layer is isoelectronic to a graphite layer and the stacking is like that of BN with a C–B–C–B sequence in adjacent layers. This gives rise to the formation of hexagonal prismatic holes, all of which are filled by Li atoms. According to the (8–*N*) rule, any compound Li_xB_xC with $0 < x \leqslant 1$ and any BC frame with a mean valency of 4 can be a valence compound. Still, only the 1:1:1 composition has been observed so far [3,5].

Hitherto, little has been known about main group borocarbides. Markovskii et al. [7–10] reported the existence of ternary compounds of beryllium, calcium, strontium, and barium with boron and carbon of various

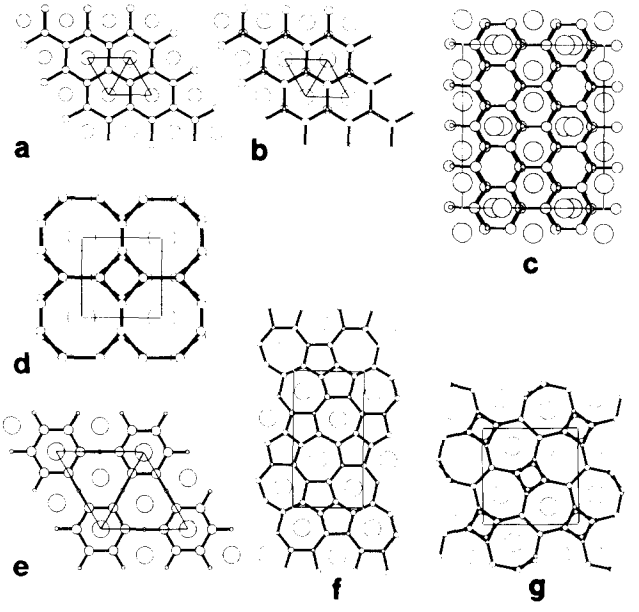

Fig. 1. Structures of metal boride and borocarbide compounds with layered flat (B, C) nets: (a) MgB_2; (b) LiBC; (c) MgB_2C_2; (d) LaB_2C_2, B and C are not distinguished owing to contradictionary reports in the literature [12,22,23]; (e) UB_2C; (f) ScB_2C_2; (g) TbB_2C (metal atoms, large circles; boron, medium circles; carbon, small circles).

composition, but there is no structural information available for compounds other than CaB_2C_2 [11] (cf. Table 1). The crystal structure is described as being isotypic to the LaB_2C_2 type [12].

Now, with MgB_2C_2, the first borocarbide of magnesium has been synthesized and characterized. In

*Corresponding author.

SSDI 0925-8388(94)01247-F

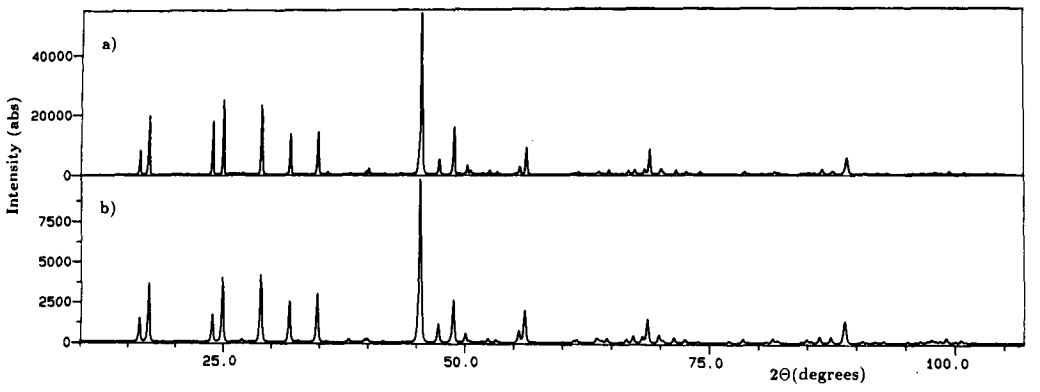

Fig. 2. (a) Experimental and (b) calculated diffraction patterns for MgB_2C_2.

Table 1
Overview of compounds with layered flat (B, C) nets. n_e = number of valence electrons per (B, C) atom. m^l = Schläfli symbol with m = ring size and l = multiplicity of ring type per ring atom; where there are differently coordinated layer atoms the m^l symbols are given in $()_n$, n being the individual multiplicity. $\bar{d}_{xy}$ = average distance within the (B, C) layers. $\bar{d}_L$ = average distance between (B, C) layers. $r_M{}^1$ = 'crystal radius' of metal atom. $r_M{}^2$ = effective ionic radius of metal ion [14]

	n_e	m^l	$\bar{d}_{xy}$ (pm)	$\bar{d}_L$ (pm)	$r_M{}^1$ (pm)	$r_M{}^2$ (pm)	References
MgB_2	4	6^3	178	352	86	72	[13]
LiBC	4	6^3	159	353	90	76	[3–5]
MgB_2C_2	4	6^3	158	374	86	72	This work
Graphite	4	6^3	142	335	–	–	[15]
LaB_2C_2	4.25	48^2	158	396	117	103	[12]
ScB_2C_2	4.25	57^2	155	344	89	75	[16]
TbB_2C	4.33	47^2	168	376	106	92	[17]
ThB_4	4	$(47^2)_4$ $(7^3)_3$	180	411	108	94	[18]
UB_2C	4.33	69^2	163	359	117	103	[19]

contrast to CaB_2C_2, which consists of 48^2 BC nets [11], it contains graphite-like $^2_\infty$[BC] layers of the 6^3 type (cf. Fig. 1). The following evaluation of the crystal structure of MgB_2C_2 shows clearly that a hypothetical CaB_2C_2 in that structure type is unfavourable for geometric reasons.

2. Experimental details

MgB_2C_2 was prepared in sealed niobium ampoules from the pure elements (magnesium: Fluka, 99.8%; α-boron: crystalline, t2N4, Johnson & Matthey; graphite: 3 ppm metal impurities, Ringsdorff). For purification purposes boron and graphite were heated to 1170 K for 5–12 h at 10^{-3} mbar. The ampoules were filled in a glove box under a purified argon atmosphere with an atom ratio of Mg:B:C = 3:1:1. The excess of magnesium is needed both as a solvent and to compensate the considerable loss of magnesium through the walls of the ampoule at the relatively high reaction temperatures. The niobium ampoules were sealed by arc welding under an argon atmosphere and placed in an argon-filled Al_2O_3 tube. To obtain single crystals suitable for X-ray structure analysis, a temperature of 1770 K was held for 10 h. The powder pattern of MgB_2C_2 is given in Fig. 2.

The excess of magnesium was removed by sublimation at 1070 K for 1 h under high-vacuum conditions. Pure-phase material was preferentially produced when relatively small ampoules (diameter = 7 mm, length = 18 mm, wall thickness = 0.7 mm) were used. Synthesis in large ampoules (diameter = 12 mm, length = 50 mm, wall thickness = 0.5 mm) generated phase mixtures (MgB_4, MgB_2, graphite) to a larger extent. Energy-dispersive X-ray analysis (EDX) with selected single crystals gave indication neither for heavier elements than magnesium nor for nitrogen or oxygen. Crystals for data collection were optically selected and checked by Buerger precession photographs. Many crystals were found to be twinned, showing diffraction patterns of pseudohexagonal metric ($a = 2184.4$, $c = 745.9$ pm) but with monoclinic intensity distributions. This observation, and the hexagonal morphology of the crystals (cf. Fig. 7), may be taken as an indication of the existence of a high-temperature phase of hexagonal symmetry.

In Fig. 3 single-crystal diffraction patterns of two individual crystals rotated by 60° are displayed. Together with a third very small crystal, rotated by 120°, the combined trilling pattern is generated. The observed trilling pattern has contributions of three crystals of different volumes (cf. Fig. 3(c)).

3. Solution and refinement of the structure

Analysis of the systematic extinctions leads to two allowed space groups, *Cmca* and *Aba2*, respectively. For the final description centrosymmetric *Cmca* was

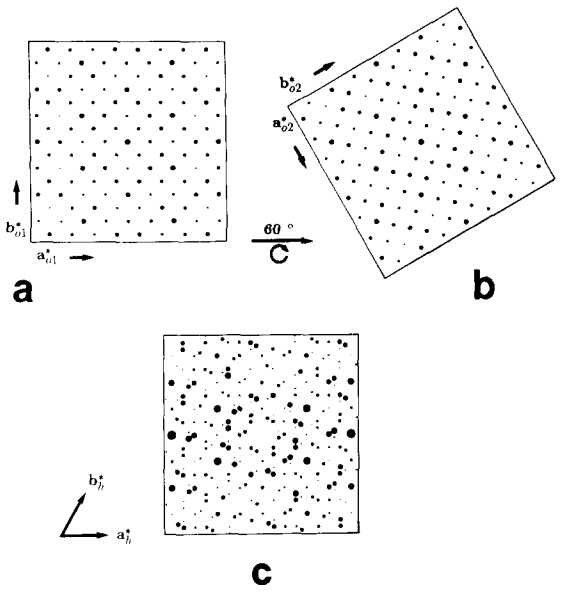

Fig. 3. Reciprocal lattice images and twinning of MgB_2C_2 crystals: projections along c. (a), (b) Unfolded intensities of two individual crystals. The third one has only a very small volume and this generates only rather weak contributions in (c). (c) Typical intensity distribution of a 60° trilling with a (001) twinning plane.

chosen, due to the occurrence of high-correlation matrix elements during refinements in *Aba*2. Even in the centrosymmetric space group the high pseudosymmetry within the nets gives rise to some, though not severe, correlations (largest element in the correlation matrix was 0.64). The structure was solved by direct methods. At the first stages of refinement all positions within the BC-nets were assigned to B atoms. During the refinement those positions with slightly higher electron density were identified as C atoms. This led to an alternating B–C distribution, which could be refined to a final reliability of $R=0.025$. To confirm the distribution of B and C within the nets other B–C patterns were investigated. In all cases, however, the resulting R-values were significantly higher and the maximal differences of the temperature factors for the substituted atoms B, C were much larger than in the final model. The final difference Fourier map contains residual electron density maxima not above 0.6 e^- $Å^{-3}$. These residuals are located close to or on the B–C bonds with significant shifts away from the centre towards the C atoms. We will come back to these features later.

If about 60 reflections which violate the extinction law for F-centering are neglected (or not observed due to a small crystal volume) then a substructure can be refined in *Fmmm* to a final R-value of 0.043. In this case, however, it is not possible to distinguish between B and C atoms, although the main features such as bond lengths and puckering of the layers are correctly reproduced. The alternation of B and C atoms is further confirmed by experimental and theoretical investigations. The density of states plots of extended Hückel calculations [22] exhibit a band gap at the Fermi level only for our final structure model [24], but not for other investigated distribution variants, which necessarily all have C–C and B–B bonds. Consistently, the temperature dependence of the electric conductivity is observed to be that characteristic of a semiconductor. Details of the X-ray data collection are listed in Table 2. Atom coordinates and temperature factors are contained in Tables 3 and 4, bond distances and angles in Tables 5 and 6.

Table 2
Crystallographic data for MgB_2C_2

Formula	MgB_2C_2
Molecular weight (g mol^{-1})	69.946
Crystal size (mm)	$0.23\times0.19\times0.08$
Crystal shape	Truncated hexagonal pyramid
Colour	Transparent dark red, silver metallic lustre
Unit cell	$a=10.922(2)$ Å, $b=9.461(2)$ Å, $c=7.459(1)$ Å
Volume ($Å^3$)	770.8(3)
Formula units per cell	16
Space group	*Cmca*-D_{2h}^{18} (No. 64)
Density ρ_{calc}, ρ_{exp} (g cm^{-3})	2.411, 2.360
μ (cm^{-1})	3.41
Temperature (°C)	25
Data collection	Four-circle diffractometer STOE STADI 4 graphite monochromator λ (MoKα) = 0.71073 Å
Scan width (°) (50 steps)	1.5 ω–θ scan, for $3°\leqslant2\theta\leqslant65°$ ω–2θ scan, for $65°\leqslant2\theta\leqslant90°$
Time intervals per step (s)	0.5–2.0
Standard reflections	0 0 4, 0 −4 −2, −4 2 2
Min./max. 2θ	$3°\leqslant2\theta\leqslant90°$
hkl range	$0\leqslant h\leqslant21$, $-18\leqslant k\leqslant18$, $-14\leqslant l\leqslant14$
No. of measured reflections	5895
No. of unique reflections	1569
$R_{int.}$	0.025
No. of reflections with $F^2>3\sigma(F^2)$	836
Structure solution	SHELXS-86 (direct methods) [20]
Refinement	SHELXS-76 [21]
No. of parameters	52
Max. shift/ESD	0.086
Max./min. peak in difference map ($eÅ^{-3}$)	0.6/−0.47
R^a	0.025
$R_w{}^b$	0.024 ($k^c=0.6251$, $g^c=0.0005$)

$$^aR=\frac{\sum(||F_o|-|F_c||)}{\sum|F_o|}.$$

$$^bR_w=\frac{(||F_o|-|F_c||\sqrt{w})}{\sum(|F_o|\sqrt{w})}.$$

$$^cw=\frac{k}{\sigma^2(F_o)+|g|\cdot|F_o|^2}.$$

Table 3
Atom coordinates and isotropic temperature factors (esd) (pm^2) for MgB_2C_2

Atom	Site	x	y	z	$U_{iso/equi}$	Occupation
Mg1	8d	0.15343(6)	0	0	65(1)	1
Mg2	8f	0	0.27981(6)	−0.0113(1)	76(1)	1
B1	8e	1/4	0.0946(2)	1/4	48(4)	1
B2	8f	0	0.5886(2)	0.2760(3)	42(5)	1
B3	16g	0.1278(2)	0.3415(1)	0.2438(2)	42(2)	1
C1	8e	1/4	0.9271(2)	1/4	44(4)	1
C2	8f	0	−0.0792(2)	0.2314(2)	46(4)	1
C3	16g	0.1245(2)	0.1750(1)	0.2231(1)	44(2)	1

Table 4
Coefficients of the anisotropic temperature factors (esd) (pm^2) for MgB_2C_2. The U_{ij} are defined for $\exp[-2\pi^2(U_{11}h^2a^{*2}+...+2U_{23}klb^*c^*)]$

Atom	U_{11}	U_{22}	U_{33}	U_{12}	U_{13}	U_{23}
Mg1	75(2)	65(2)	54(2)	0	0	1(2)
Mg2	92(2)	77(2)	58(3)	0	0	4(2)
B1	45(9)	41(7)	56(6)	0	−2(5)	0
B2	39(10)	35(7)	51(6)	0	0	−6(5)
B3	38(5)	28(4)	61(4)	−4(4)	4(4)	4(4)
C1	29(8)	29(6)	74(6)	0	−3(5)	0
C2	28(9)	30(7)	78(6)	0	0	4(4)
C3	31(4)	27(3)	72(4)	−1(4)	−4(4)	−1(3)

4. Crystal structure

The structure of MgB_2C_2 contains graphite-like but slightly puckered $^2_\infty[BC]^-$ layers whose charge is counterbalanced by the Mg^{2+} cations (Figs. 4, 6(a)). The mutual coordination of boron and carbon consists of five atoms of the other type, three of which are in the same and two in adjacent layers. The puckering leads to a maximum deviation of 20 pm (for C3) from the optimized plane. The BC distances within the nets are in the range from 156.2 to 159.5 pm. These values are comparable to that found in LiBC, which shows a BC distance of 158.9 pm. If the single-bond radii of B and C are taken to be 85 and 77 pm [25] a bond length of d(B–C) = 162 pm is expected for a single bond. The observed distance is somewhat shorter but not as short as one would expect for a bond order of 1.33 [25] as in graphite, where the shortening compared to a C–C single bond is 7.8%. Such a shortening should lead to a B–C bond length of about 149 pm in MgB_2C_2 and LiBC. On the other hand, in MgB_2 the observed B–B distance is 178 pm, which is longer than a B–B single bond of 170 pm. These findings may be explained by an elongation of the bond lengths due to the increasing negative charge of the nets in the order graphite, MgB_2C_2 and MgB_2. The distance between two graphite-like layers is influenced as well by the charge of the nets as by the Coulomb interaction with the cations. Less effective shielding of the negative charge due to fewer cations between the layers may be responsible for the larger average layer distance in MgB_2C_2 compared to MgB_2 and LiBC. LiBC and MgB_2 have nearly the same interlayer distance, despite their differently charged layers (cf. Table 1). Having the same number of cations and anions in both compounds, the Coulomb interaction in MgB_2 must be larger, thus compensating the interlayer repulsion, because of the higher cation charge.

Attempts to calculate deformation density distributions especially for the BC net were not really satisfying. Diffraction data have been collected up to $2\theta = 90°$ but the X–X deformation density plots show some features which must be attributed to data errors. Still there are some observations which are quite useful and which support our description of the compound as an intercalated graphite-related structure. In Fig. 5 parts of the [BC] net are displayed together with an iso-density surface of 0.29 e^- $Å^{-3}$. It should be noted that there is considerable deformation density only along the net. Within the hexagonal linkage the density shows a clear tendency to be close to those positions which we found to be best suited for carbon atoms. Furthermore there is some indication that a certain π-bonding character is present because of the elongation of the iso-surfaces perpendicular to the [BC] plane.

Each of the magnesium cations is coordinated by six boron and six carbon atoms, forming slightly distorted hexagonal prisms. Surprisingly, the cations are not uniformly distributed between the $[BC]^-$ layers but concentrated in certain spatial regions (Figs. 4(a), 6(a)). They show local 'clustering' of four Mg atoms which

Table 5
Selected interatomic distances d (esd) (pm) for MgB_2C_2 (n denotes the frequency)

Atom/pair	d	n
Mg1–C1	225.07(7)	2
Mg1–B1	232.18(8)	2
Mg1–C3	236.86(9)	2
Mg1–B3	244.5(1)	2
Mg1–B2	251.0(2)	2
Mg1–C2	252.0(1)	2
Mg1–Mg2	313.42(8)	2
Mg1–Mg1	335.2(1)	
Mg2–B2	233.4(2)	
Mg2–C3	242.7(2)	2
Mg2–B3	243.1(2)	2
Mg2–C3	244.1(2)	2
Mg2–C2	247.8(2)	
Mg2–C2	250.9(2)	
Mg2–B2	252.1(2)	
Mg2–B3	257.0(2)	2
Mg2–Mg1	313.42(8)	2
Mg2–Mg2	377.19(5)	2
Mg2–Mg2	417.0(1)	
B1–C3	158.0(2)	2
B1–C1	158.5(3)	
B1–Mg1	232.18(8)	2
B1–C1	373.51(5)	2
B2–C3	158.7(2)	2
B2–C2	158.9(3)	
B2–Mg2	233.4(2)	
B2–Mg1	251.0(2)	2
B2–Mg2	252.1(2)	
B2–C2	339.8(3)	
B2–C2	406.3(3)	
B3–C1	156.2(2)	
B3–C3	158.3(1)	
B3–C2	159.5(2)	
B3–Mg2	243.1(2)	
B3–Mg1	244.5(1)	
B3–Mg2	257.0(2)	
B3–C3	357.9(2)	
B3–C3	388.7(2)	
C1–B3	156.2(2)	2
C1–B1	158.5(3)	
C1–Mg1	255.07(7)	2
C1–B1	373.51(5)	2
C2–B2	158.9(3)	
C2–B3	159.5(2)	2
C2–Mg2	247.8(2)	
C2–Mg2	250.9(2)	
C2–Mg1	252.0(1)	2
C2–B2	339.8(3)	
C2–B2	406.3(3)	
C3–B1	158.0(2)	
C3–B3	158.3(1)	
C3–B2	158.7(2)	
C3–Mg1	236.86(9)	
C3–Mg2	242.7(2)	
C3–Mg2	244.1(2)	
C3–B3	357.9(2)	
C3–B3	388.7(2)	

Table 6
Selected angles (esd) for MgB_2C_2 (degrees)

Atoms	Angles	n
C3–B1–C3	122.5(2)	
C3–B1–C1	118.77(8)	2
C3–B2–C3	118.0(2)	
C3–B2–C2	121.00(8)	2
C1–B3–C3	122.6(2)	
C1–B3–C2	120.0(1)	
C3–B3–C2	117.3(2)	
B3–C1–B3	117.5(2)	
B3–C1–B1	121.23(8)	2
B2–C2–B3	118.29(8)	2
B3–C2–B3	122.1(2)	
B1–C3–B3	116.5(2)	
B1–C3–B2	119.7(1)	
B3–C3–B2	122.1(2)	

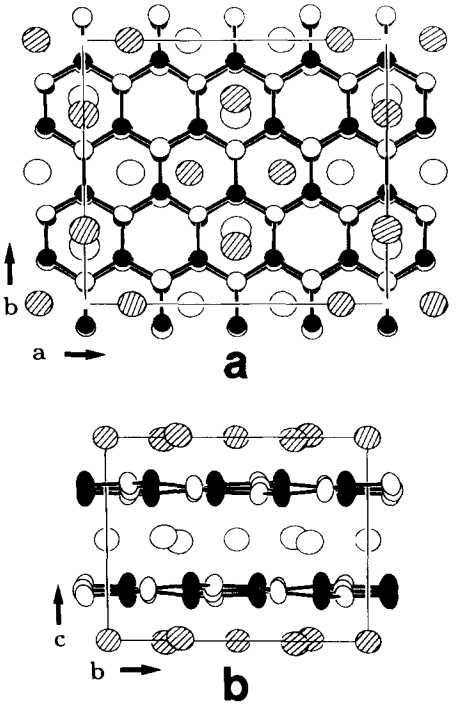

Fig. 4. Crystal structure of MgB_2C_2: (a) [001] view (boron, small black circles; carbon, small open circles; magnesium, large circles) with different shading of the Mg atoms at different height; (b) puckering of the [BC] layers in a [100] projection.

are surrounded by non-occupied hexagonal prismatic voids. Only half of these voids formed by the BC layers are occupied. The others may serve as open sites for intercalation atoms or to enable cation mobility. The Mg groups in adjacent layers are shifted in such a way that a configuration as displayed in Fig. 6(b) (lower right part) results. It should be noted that the shifting of the Mg clusters between adjacent [BC] double layers is not such that all hexagonal B_6C_6 prism stacks are filled. Some remain open throughout the whole structure

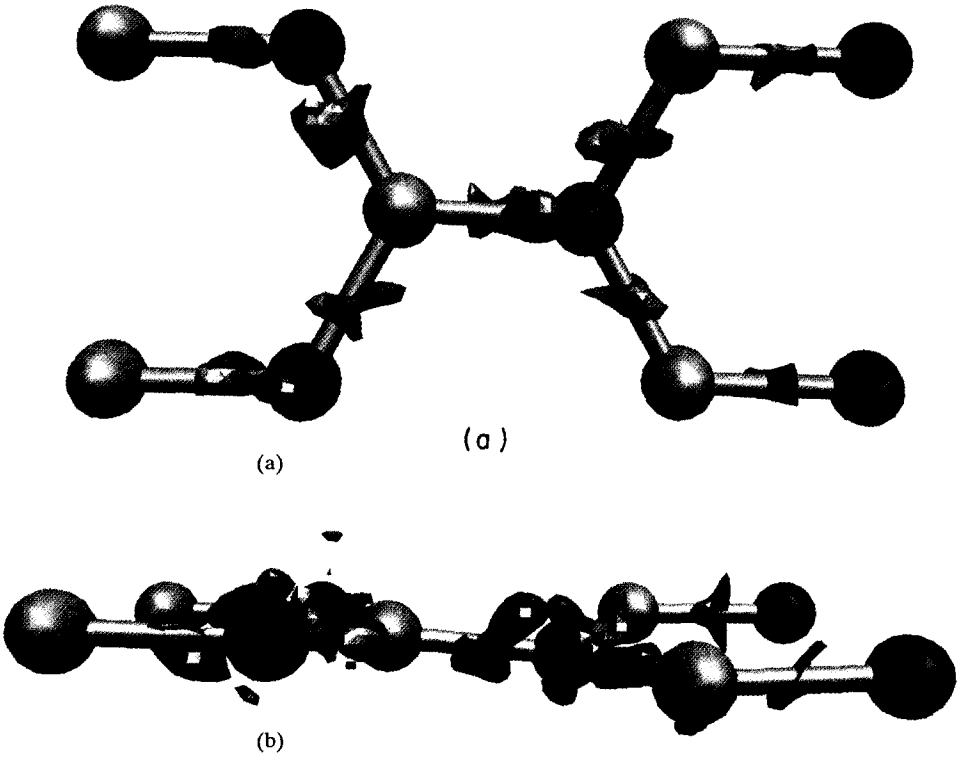

Fig. 5. Deformation density plots of a selected part of the MgB_2C_2 structure (B, grey; C, black). The iso-density surface displays the course of $\rho(r)=0.29$ e^{-1} Å^{-3}. View (a) perpendicular to and (b) along the [BC] layer.

(cf. Fig. 6(b) completely open hexagons in the lower right part).

Inspection of the Mg_4 groups in Fig. 6(a) reveals that the Mg atoms repel each other considerably. All of them are shifted outwards from the centre of the group. Assuming an equivalent shift for the outer empty prisms were they to be used by Mg^{2+} makes it clear that they can no longer be occupied.

The pattern of filled prisms in Fig. 6(b) (left-hand side) is markedly different from that of the empty ones. Hence, there is no possibility of distributing the Mg_4 groups in the next layer over only empty prisms of the previous one. Consequently, the layering must lead to adjacent occupied prisms along the [001] direction. However, there is no need for stacks of empty prisms throughout the structure along this direction. The shortest translation for occupation of all prism stacks with the Mg_4 arrangement gives rise to a three-layer stacking. This, however, has a much larger number of occupied neighbouring prisms than the observed structure. Still there is a two-layer arrangement which yields only half the number of completely filled $Mg(BC)_6$ prism stacks (cf. Fig. 6(b), upper right part). At the first glance, there is no obvious reason why this one should not be more or as stable than the real structure. Its corresponding primitive unit cell would even be smaller.

Trying to solve the general problem of distributing a set of slightly too large or too highly repulsing atoms on twice the number of positions, we found only three reasonable solutions of prism clustering, namely the M_4, M_6 and M_8 groups and two chain solutions. We rejected the M_5 and the M_7 case because of the very large resulting unit cells. For the M_6 case (cf. Fig. 6(d)) an opening of one prism in the centre is the only solution; and a hypothetical M_9 arrangement (cf. Fig. 6(f)) would have three empty prisms in the middle and therefore be too open to fulfil stoichiometry. Consequently the M_8 cluster has an opening of two six-rings in the centre (cf. Fig. 6(e)). The investigated cases are listed in Table 7, where the ratios of filled to open prisms are given in column R_1. Only the cases M_4, M_6 and M_8 yield 1:1 ratios as given by the stoichiometry MgB_2C_2 and by the basic structure principle, namely the intercalation of graphite-like layers stacked on top of each other. The three M_3 cases of highest symmetry which have been found are shown in Fig. 6(c) with the primitive unit cells outlined in bold black. Clearly, there is no possibility to yield $R_1=1$, and hence we did not inspect possible stacking sequences here. The M_6 case in Fig. 6(d) yields a beautiful highly symmetric solution even for the stacking of two consecutive layers (Fig. 6(d), right-hand side). Indeed, this may be the structure of the suspected high-temperature phase.

A slightly larger unit cell is found for the M_8 (cf. Fig. 6(e)) case with a lot of different stacking possibilities even for two layers. Here, however, we find three filled

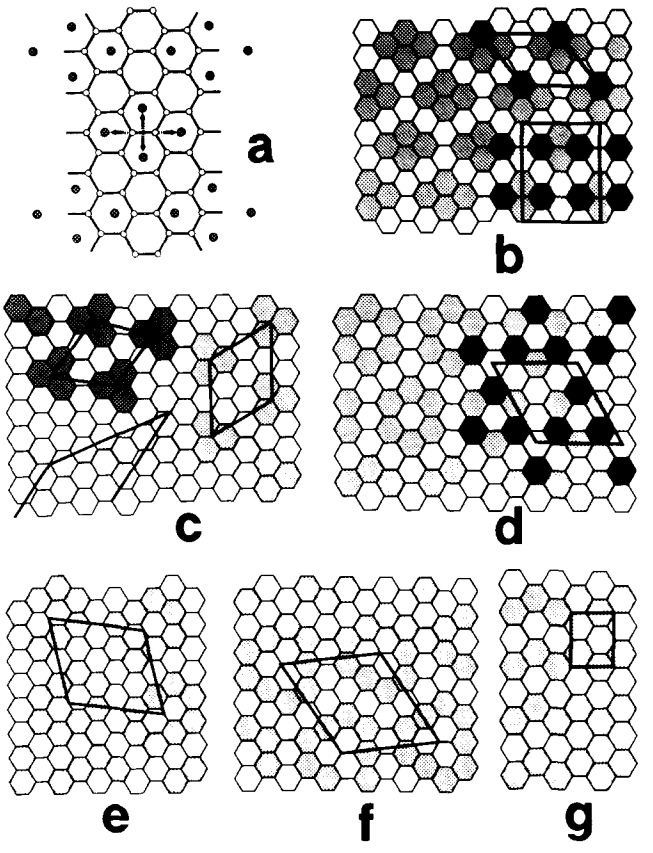

Fig. 6. Observed and alternative cation distribution in the hexagonal prisms between the [BC] layers. (a) Shift of the Mg^{2+} cations away from the centre of an Mg_4 unit because of repulsive interactions, as observed. This effect favours a corona of open prisms around the Mg_4 moiety. (b) Schematic representation of filled (shaded or black) and unfilled (not shaded) prisms. On the left-hand side the filling pattern of one cation layer is shown, and on the right two possibilities of two-layer stacks are shown together with the smallest resulting unit cells (shadings discriminate the two layers, full black hexagons denote consecutively filled prisms in the projection direction). In the lower right part the observed filling pattern is shown. (c) The three simplest and most compact M_3 distributions, all of which cannot fulfil the ratio $R_1 = 1$ (cf. Table 7). (d) Hexagonal rings solution M_6 with the correct ratio $R_1 = 1$ and a good two-layer stacking (compare with left- and right-hand side of (b)). (e) Eight-ring arrangement M_8 without two-layer stacking models because of numerous possibilities. (f) Nine-ring model M_9, which cannot meet the $R_1 = 1$ requirement. (g) Zig-zag chain distribution, M_n being the only model which never fills consecutive prisms along [001]. In (f) and (g) three consecutive filled prisms in a line cannot be avoided, which should be unfavourable in terms of repulsion.

prisms in a line, which does not seem to be preferable on the basis of the previous discussion. Thus the M_8 model is not considered to be a good solution. The M_9 clustering does not lead to the correct ratio for R_1 and has the same disadvantage as M_8. Finally, there is a remarkable chain solution M_n which obviously meets all the previously discussed conditions (cf. Fig. 6(g)). There is even a two-layer stacking possible without having consecutively filled prisms. It is not yet clear why the observed structure (Fig. 6(b), lower right side) is the most stable one at room temperature, because there is no good straightforward argument against the M_6 and the M_n models.

Table 7
Geometric properties of different Mg distributions in the B_2C_2 partial structure. Case refers to Fig. 6, n_{clust} is the number of directly neighboured Mg atoms, n_{surr} the number of unoccupied surrounding prisms and n_{surr}^{eff} the corresponding effective number applying crystallographic multiplicity. The total number of prisms per unit cell is n_6^{cell} while the ratio of occupied and unoccupied prisms is given under R_1. If $R_1 \neq 1$ the stoichiometry requirement is not fulfilled

Case	n_{clust}	n_{surr}	n_{surr}^{eff}	n_6^{cell}	R_1
c	3	9	$\frac{6}{3}+\frac{3}{2}$	7	1:0.75
b	4	10	$\frac{6}{3}+\frac{4}{2}$	16	1:1
d	6	13	$\frac{6}{3}+\frac{6}{2}+1$	12	1:1
e	8	16	$\frac{14}{2}+2$	18	1:1
f	9	18	$\frac{6}{3}+\frac{9}{2}+3$	19	1:1.11
g	∞	∞	$\frac{2}{2}$	4	1:1

5. Properties

MgB_2C_2 crystallizes with pyramids (Fig. 7) of silvery lustre, but is transparent to visible light with a dark red colour. The compound is relatively hard but has a preferred cleavage plane perpendicular to the [001] direction. The electric conductivity exhibits a semiconducting behaviour from 4 K to room temperature. No significant variation of the stoichiometry with respect to further substitution of C by B^- according to $(Mg_{1+x}B_{2+2x}C_{2-2x})$, and vice versa, which should have an effect on the lattice constants, was observed by means of powder diffraction studies. The experimental density was averaged from six independent pycnometric measurements. As is generally expected, it is slightly smaller (2%) than the theoretical one.

Even small crystals of MgB_2C_2 are seemingly inert against diluted acids for several days, but decompose instantaneously in concentrated nitric acid. In contrast to graphite, this compound is much more stable against liquid bromine at room temperature. A differential thermal analysis (DTA) of a mixture of MgB_2C_2 with Li exhibits an exothermal peak at 550 K. The powder diffraction diagrams of such products show in addition to lines of lithium some broad lines, which can be assigned to LiBC.

The voids in the Mg^{2+} layers may well enhance topochemical reactions as positions for intercalating

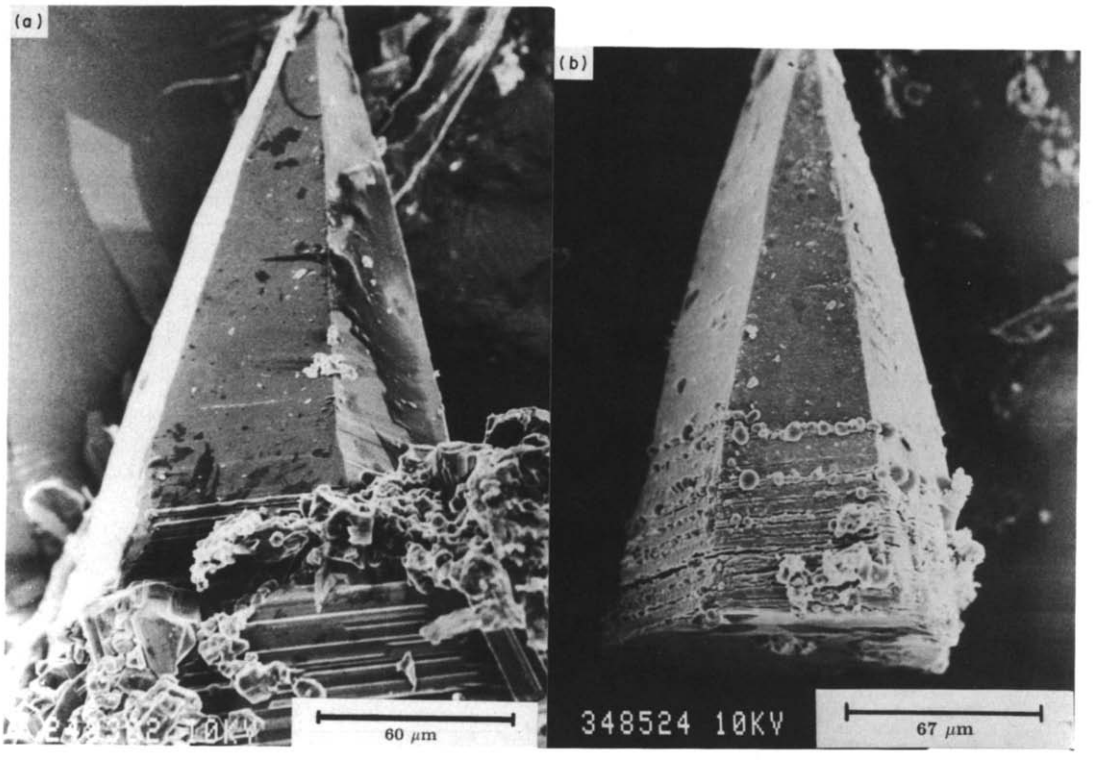

Fig. 7. (a) Scanning electron microscope picture of an MgB_2C_2 single crystal. The hexagonal pyramidal crystal clearly shows steps on the surface, which may be due to stacking faults and domain formation. (b) The same crystal after exposure to air for about half a year. The topochemical character of the hydrolysis reaction is clearly visible. Seemingly the reaction starts at stacking faults, e.g. steps on the surface of the crystal.

additional chemical species and as mobility promoters for deintercalation procedures. From the Coulomb potential distribution to void positions are not suitable for large or highly charged cations; they may accommodate small anions better. This, however, must be accompanied by a *p*-type doping of the layers and/or an exchange of Mg^{2+} against trivalent metal ions M^{3+}. The observed uptake of lithium, however, shows that small metal atoms may diffuse into the structure.

The occurrence of twinned crystals of MgB_2C_2 with pseudohexagonal metric indicates the existence of a more symmetric arrangement at higher temperatures. We anticipate that at higher temperatures the compound will be a good ionic conductor. Even at room temperature MgB_2C_2 exhibits a much better ionic conductivity than LiBC. This can be traced back to the existence of voids in the Mg substructure.

Acknowledgements

We thank Dr. V. Shklover for the preparation of the SEM pictures, M. Spahr and C. Mensing for electric and magnetic measurements. The financial support by the Swiss National Science Foundation (projects 21-36586.92 and 4030-032775) is gratefully acknowledged.

References

[1] D. O'Hare, in D.W. Bruce and D. O'Hare (eds.), *Inorganic Materials,* Wiley, 1992, pp. 165–233.
[2] H.O. Grimm and A. Sommerfeld, *Z. Phys., 36* (1926) 36.
[3] G. Mair, *Dissertation,* Max-Planck-Institut, Stuttgart, 1984.
[4] R. Nesper, *Prog. Solid State Chem., 20* (1990) 1.
[5] M. Wörle and R. Nesper, unpublished results.
[6] J. Kouvetakis, R.B. Kaner, M.L. Sattler and N. Bartlett, *J. Chem. Soc. Chem. Commun.,* (1986) 1758.
[7] R.Y. Markovskii and N.V. Vekshina, *J. Appl. Chem. USSR, 34* (1961) 236.
[8] N.V. Vekshina and R.Y. Markovskii, *J. Appl. Chem. USSR, 35* (1962) 23.
[9] R.Y. Markovskii and N.V. Vekshina, *J. Appl. Chem. USSR, 37* (1964) 2107.
[10] R.Y. Markovskii, N.V. Vekshina, Y.D. Kondrashev and I.M. Stroganova, *J. Appl. Chem. USSR, 39* (1966) 10.
[11] T. Breant, D. Pensec, J. Bauer and J. Debuigne, *C.R. Acad. Sci. Ser. C, 287 C* (1978) 261.
[12] J. Bauer and O. Bars, *Acta Crystallogr., B36* (1980) 1540.
[13] R.Y. Markovskii, N.V. Vekshina, Y.D. Kondrashev and T.K. Voevodskaya, *J. Appl. Chem. USSR, 44* (1971) 970.
[14] R.D. Shannon, *Acta Crystallogr., A32* (1976) 751.
[15] P. Trucano and R. Chen, *Nature, 258* (1975) 136.
[16] G.S. Smith, Q. Johnson and P.C. Nordine, *Acta Crystallogr., 19* (1965) 668.
[17] J. Bauer and J. Debuigne, *J. Inorg. Nucl. Chem., 37* (1975) 2473.
[18] A. Zalkin and D.H. Templeton, *Acta Crystallogr., 6* (1953) 269.
[19] R. Rogl, J. Bauer and J. Debuigne, *J. Nucl. Mater., 165* (1989) 74.

[20] G.M. Sheldrick, SHELXS-86. A progam for crystal structure solution, in G.M. Sheldrick, C. Krüger and R. Goddard (eds.), *Crystallographic Computing 3*, Oxford University Press, Oxford, 1985, pp. 175–189.

[21] G.M. Sheldrick, SHELX-76. Program for crystal structure determination, University of Cambridge, 1976, unpublished.

[22] J.K. Burdett, E. Canadell and T. Hughbanks, *J. Am. Chem. Soc., 108* (1986) 3971.

[23] P.K. Smith, *Ph.D. Thesis,* University of Kansas Lawrence, Kansas, 1964.

[24] M. Wörle and R. Nesper, to be published.

[25] L. Pauling, *The Nature of the Chemical Bond,* Cornell University Press, Ithaca, New York, 1960.